

Numerical Study on Combustion Characteristics of Spray Flat Flames

Time-dependent Burning Behavior of Polydisperse Spray Entering Gaseous Flame Front

*Fumiteru AKAMATSU, Hiroyasu SAITOH, and Masashi KATSUKI
Department of Mechanical Engineering, Osaka University
2-1 Yamadaoka, Suita, Osaka 565-0871, Japan

ABSTRACT Numerical calculations and experimental observations were conducted on combustion processes of n-decane polydisperse spray entering gaseous flat-flame stabilized in laminar 2D counter flow configuration. The both results are compared to each other to ensure validity of the simulation model. The Eulerian/Lagrangian approach was used for the numerical simulations. For the gaseous phase, Navier-Stokes equation together with mass, energy and species conservation equations was solved based on the finite control volume method with SIMPLE algorithm. Transport properties and thermodynamic data of the gaseous species were obtained from CHEMKIN. For the disperse phase, all the individual droplets were tracked without using the concept of "droplet parcel". The film theory was employed for estimating the droplet evaporation rate and the heat transferred from the gaseous phase to the droplet interior. Time evolution of burning processes of fuel spray entering high temperature region of the gaseous flame was discussed. As a result, twin flames of premixed combustion of pre-vaporized fuel and diffusion combustion of droplet groups were observed on the spray flow side.

Key Words: Spray Combustion, Flame Structure, Numerical Simulation, and Film Theory

1. INTRODUCTION

Spray flames are complicated reacting turbulent phenomena in which fuel atomization, droplet dispersion into gaseous phase, evaporation, mixing of fuel vapor with air, and so on occur simultaneously, interacting each other. Therefore, the flame structure is very complicated. In addition, on the experimental measurements, the use of intrusive probes into flames is very limited due to the existence of liquid droplets. Besides, the advanced laser diagnostics commonly used for gaseous fuel flames are not always applicable owing to intense Mie scattering from droplets. Therefore, there still exist many unrevealed characteristics of spray flames.

In early 1970's, Chiu et al., proposed the droplet group combustion theory⁽¹⁾ in which droplet collective effect on the flame structure was taken into account. We have shown recently the quantitative experimental verification of the droplet group combustion by using the spatially and temporally resolved multi-component data of combustion reactions and spray characteristics⁽²⁻⁴⁾ in stead of ordinary time-averaged data. The experiments revealed that spray flames have much more complicated structure than they were modeled in the initial concept of the droplet group combustion. Spatial nonuniformity of spray tends to form droplet groups, and temporal and spatial variations of their behavior generate the change in flame structure.

Since it is impossible at present to measure all the physical quantities in spray flames experimentally, more precise comparison of the experimental results and the numerical calculation results is essential to further elucidate the detailed spray flame structure and to build-up a comprehensive simulation model of spray combustion. However, due to the lack of experimental information, most of the spray combustion models in the past did not always reflect real physics of spray combustion. Therefore, it is necessary to build a spray combustion model based on the

physics with deep communication between experimental and numerical researches.

For the first trial in the present project, numerical calculations and experimental observations⁽⁵⁾ were carried out on combustion processes of n-decane polydisperse spray entering gaseous flat-flame stabilized in laminar 2D counter flow configuration. The results were compared to each other to ensure validity of the simulation model. Navier-Stokes equation, together with mass, energy and species conservation equations was solved for the gaseous phase, considering the temperature dependence of transport properties and thermodynamic data of the gaseous species. For the disperse phase, all the individual droplets were tracked without using the concept of "droplet parcel". The film theory was employed for estimating the droplet evaporation rate and the heat transferred from the gaseous phase to the droplet interior. Detailed time-dependent burning processes of polydisperse fuel spray entering the gaseous flame front were discussed.

2. CALCULATION METHOD

The planar two-dimensional flow field for the calculation is shown in Fig. 1. The origin of the calculation domain was located at the center of the upper rectangular burner port, from which liquid fuel, n-decane ($C_{10}H_{22}$) was supplied. The geometry of the burner port was 20 mm in width and the port separation was 20 mm. From the upper port, atmospheric air ($T=300K$, $P=0.1013MPa$, and oxygen mass fraction $Y_{O_2}=0.2357$) was issued at the velocity of 0.4 m/s. From the lower port, pre-mixture of atmospheric air and n-decane vapor (equivalence ratio, $\phi_g = 0.6$) was issued in the region of $0 \leq y \leq 3mm$, and atmospheric air was issued in the region of $3 < y \leq 10mm$ at the velocity of 0.4 m/s. The gaseous flame was stabilized in a laminar counterflow, stretch ratio of which is 40 1/s.

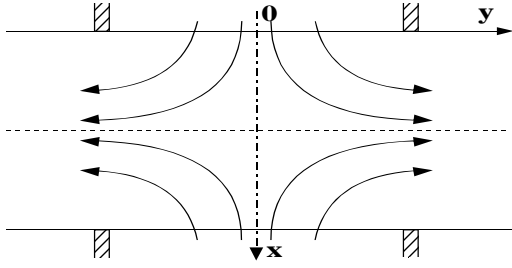


Fig. 1 Schematic of the flow field.

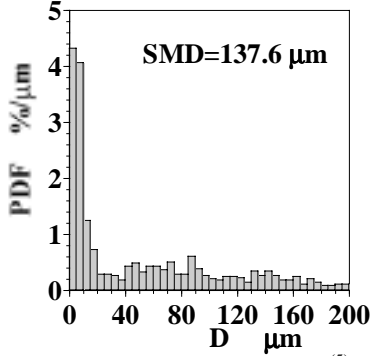


Fig. 2 The droplet size distribution⁽⁵⁾ used for the calculation.

At a moment, $t = 0$ ms, polydisperse n-decane spray injection was started to flow from the upper port in the region of $0 \leq y \leq 3\text{mm}$ at the velocity of 0.4 m/s. The fuel-air mass ratio of the central ($0 \leq y \leq 3\text{mm}$) premixed spray was $0.016 \text{ kg}_{\text{fuel}}/\text{kg}_{\text{air}}$, which corresponds to bulk equivalence ratio, $\phi_f = 0.237$. Droplet size distribution used for the calculation is shown in Fig. 2. This was obtained by PDA measurement in the corresponding experiment⁽⁵⁾ of this numerical calculation in the non-reacting condition. The initial position of droplet was determined by stochastic processes to generate a uniform spray flow in the region of $0 \leq y \leq 3\text{mm}$ of the upper port.

Gaseous species considered in the calculations were O_2 , N_2 , CO_2 , H_2O , and $\text{C}_{10}\text{H}_{22}$. Their transport properties and thermodynamic data were obtained by CHEMKIN^(6,7). Properties of liquid n-decane were obtained from the Ref. (8). The governing equations considered for the gaseous phase were mass, momentum, energy, and species mass balances.

For time-dependent planar two-dimensional flows, these equations can be written in a general form using a dependent variable, ψ

$$\frac{\partial \rho \psi}{\partial t} + \frac{\partial}{\partial x} (\rho u \psi - \Gamma \frac{\partial \psi}{\partial x}) + \frac{\partial}{\partial y} (\rho v \psi - \Gamma \frac{\partial \psi}{\partial y}) = S_\psi + S_{l,\psi} \quad (1)$$

where ρ is the gaseous phase density, u and v the gaseous phase velocity in the x and y direction, respectively, Γ the transport coefficient, and S_ψ the source term. Additional source term, $S_{l,\psi}$, was considered to take interaction between the gaseous and disperse droplet phases into account. The gaseous phase density, ρ , is calculated from the state equation of the ideal gas. The particular expressions for $S_\psi + S_{l,\psi}$ and Γ pertaining to each dependent variable are shown in Table 1, where h is the specific total enthalpy, μ the viscosity, Pr the Prandtl number, Sc the Schmidt number, P the static pressure, g the

Table 1 Transport coefficients and source terms in equation (1).

	ψ	Γ	$S_\psi + S_{l,\psi}$
1	1	0	$S_{l,m}$
2	u	μ	$-\frac{\partial P}{\partial x} + \frac{\partial}{\partial x} \mu \frac{\partial u}{\partial x} + \frac{\partial}{\partial y} \mu \frac{\partial v}{\partial x} + \rho g + S_{l,u}$
3	v	μ	$-\frac{\partial P}{\partial y} + \frac{\partial}{\partial x} \mu \frac{\partial u}{\partial y} + \frac{\partial}{\partial y} \mu \frac{\partial v}{\partial y} + S_{l,v}$
4	h	μ/Pr	$S_{l,h}$
5	Y_k	μ/Sc	$S_{combu,k} + S_{l,Y_k}$

gravitational acceleration, $S_{combu,k}$ the source term with the combustion. These governing equations were discretized by the finite volume method using SIMPLE algorithm⁽⁹⁾ for solving the static pressure.

Mass, heat and momentum interchanges between the gaseous and disperse phases were calculated by the method of PSI-Cell model⁽¹⁰⁾ in which all interactions are evaluated on the basis of the gaseous phase calculation grids and its control volume. Interaction terms between the phases during a calculation time step are assumed to be concentrated at a control volume of the droplet final location of the time step. The followings are assumptions for the droplets.

- 1) No collision and no breakup of droplets occur.
- 2) Droplets are spherical and have uniform internal properties.
- 3) Volume of droplets is negligible.

The interaction terms between the gaseous and disperse phases were calculated explicitly regardless the implicit calculation of the gaseous phase.

The equation describing a droplet motion is expressed as follows,

$$m_i \frac{d\mathbf{V}_i}{dt} = \mathbf{F} + m_i \cdot \mathbf{g} \quad (2)$$

where $\mathbf{F}=(F_x, F_y)$ is a drag force acting on a droplet by the gaseous phase expressed as follows,

$$\mathbf{F} = \frac{1}{8} \pi d_i^2 \rho (\mathbf{V} - \mathbf{V}_i) |\mathbf{V} - \mathbf{V}_i| C_D \quad (3)$$

where d_i is the droplet diameter, ρ the gaseous phase density, $m_i = (\pi/6) \cdot d_i^3 \rho_i$ the droplet mass, ρ_i the droplet density, $\mathbf{V}=(u, v)$ the gaseous phase velocity vector, $\mathbf{V}_i=(u_i, v_i)$ the droplet velocity vector, $\mathbf{g}=(g, 0)$ gravitational acceleration vector. The drag coefficient of a droplet, C_D , is expressed as follows⁽¹¹⁾,

$$C_D = \frac{24}{Re_d} \left[1 + \frac{Re_d^{2/3}}{6} \right] \quad (4)$$

where Re_d is a droplet Reynolds number expressed as follows.

$$Re_d = \frac{\rho |\mathbf{V} - \mathbf{V}_i| d_i}{\mu} \quad (5)$$

One of the most important issues in spray flame simulations is a droplet evaporation model. In the most

simplified case, it is assumed that no evaporation occurs prior to the saturation temperature of liquid fuel droplet. In the present study, for estimating the evaporation rate below the saturation temperature, the film theory⁽⁸⁾ was adopted. It is assumed that resistance to the heat and mass exchange between the droplet surface and the gaseous flow is concentrated within an imaginary gas film of constant thickness. To estimate the temperature and the physical properties of the mixture in the film, so-called the 1/3 rule⁽¹²⁾ was used,

$$T_f = T_l + A(T - T_l), \quad Y_{Ff} = Y_{Fs} + A(Y_F - Y_{Fs}) \quad (6)$$

where T_f is reference temperature in the film, T_l the droplet temperature, A the constant factor ($=1/3$, in this study), T the gaseous phase temperature in the surroundings of the droplet, Y_{Ff} the mass fraction of fuel vapor in the film, Y_{Fs} the mass fraction of fuel vapor at the droplet surface, Y_F the mass fraction of fuel vapor in the surroundings of the droplet.

Based on the film theory, the droplet evaporation rate, \dot{m}_l , and the heat transferred to the droplet interior from the gaseous phase, Q_l , are expressed in the following relations⁽⁸⁾, respectively,

$$\dot{m}_l = \pi d_l \rho_f D_f Sh^* \ln(1 + B_M) \quad (7)$$

$$Q_l = \dot{m}_l \left[\frac{C_{pFf}(T - T_l)}{B_T} - L(T_l) \right] \quad (8)$$

where ρ_f is the mixture density in the film, D_f the mixture diffusion coefficient in the film, C_{pFf} the fuel vapor specific heat at constant pressure in the film, $L(T_l)$ the latent heat of the vaporization at the droplet temperature T_l . B_M is the Spalding's mass transfer number defined as follows.

$$B_M = \frac{Y_{Fs} - Y_F}{1 - Y_{Fs}} \quad (9)$$

B_T is the Spalding's heat transfer number obtained by the following equations,

$$B_T = (1 + B_M)^\theta - 1 \quad (10)$$

$$\theta = \frac{C_{pFf}}{C_{pf}} \frac{Sh^*}{Nu^*} \frac{1}{Le_f} \quad (11)$$

where Le_f and C_{pf} are the Lewis number and the specific heat at constant pressure of the mixture in the film, respectively. Sh^* and Nu^* are the modified Sherwood and Nusselt number of the film, respectively, defined as follows⁽¹³⁾.

$$Sh^* = 2 + \frac{(1 + Re \cdot Sc)^{1/3} [\max(1, Re_d)]^{0.077} - 1}{F(B_M)} \quad (12)$$

$$Nu^* = 2 + \frac{(1 + Re \cdot Sc)^{1/3} [\max(1, Re_d)]^{0.077} - 1}{F(B_T)} \quad (13)$$

$$F(B) = (1 + B)^{0.7} \frac{\ln(1 + B)}{B} \quad (14)$$

Accordingly, equations describing the diameter and temperature changes of a droplet are expressed as follows,

$$\frac{dd_l}{dt} = - \frac{2\dot{m}_l}{\pi d_l^2 \rho_l} \quad (15)$$

$$\frac{dT_l}{dt} = \frac{Q_l}{(1/6)\pi d_l^3 \rho_l C_{pl}} \quad (16)$$

where C_{pl} is the specific heat of the liquid fuel droplet.

The source terms, $S_{i,\phi}$, by interactions between the gaseous and disperse phases are expressed using the total number of droplets, N , existing in each control volume of gaseous phase calculation grid. For the equation of the mass balance,

$$S_{i,m} = \frac{\sum \dot{m}_l}{\Delta V} \quad (17)$$

For the equation of the momentum,

$$S_{i,u} = - \frac{\sum F_x}{\Delta V}, \quad S_{i,v} = - \frac{\sum F_y}{\Delta V} \quad (18)$$

For the equation of the energy,

$$S_{i,h} = \frac{\sum (\dot{m}_l h_f(T) - Q_l - \dot{m}_l (C_{pF}(T - T_l) + L(T_l)))}{\Delta V} \quad (19)$$

For the equation of the species balance,

$$S_{i,y_k} = \delta_{F,k} \frac{\sum \dot{m}_l}{\Delta V} \quad (20)$$

where ΔV is volume of the control volume, δ the Kronecker's delta, $h_f(T)$ the specific enthalpy of the fuel vapor at the gaseous phase temperature, T .

For the combustion reaction model, one-step global reaction of n-decane was adopted⁽¹⁴⁾. The source term, $S_{combu,k}$, in the equations of species conservation is expressed using the combustion reaction rate per unit volume, R_F , as follows,

$$S_{combu,k} = - \frac{n_k}{n_F} \cdot \frac{W_k}{W_F} \cdot R_F \quad (21)$$

where n_k is the molar stoichiometric coefficient of the k 's species of the one-step global reaction (positive for the production side), and W_k is the molecular weight of k 's species.

For the calculation, planar symmetry on the central plane ($y = 0$) associated with mirror boundary condition was assumed. The calculation domain ($0 \leq x \leq 20 \text{ mm}$, $0 \leq y \leq 10 \text{ mm}$) was divided into 157×77 equally spaced computational grids in the x and y directions, respectively, (which corresponds to the actual control volume size of $130 \mu\text{m} \times 130 \mu\text{m}$). The calculation time step was 0.1 ms.

3. RESULTS and DISCUSSION

Figure 3 to 7 show calculation results at $t = 5, 25, 30, 35,$ and 40 ms , respectively, after the spray injection and the corresponding flame photograph at each calculation time step (the figure (d)) obtained in the corresponding experiment⁽⁵⁾. In the figure (a), the gaseous phase velocity vectors, $\mathbf{V} = (u, v)$, superimposed on 2-D profile of the gaseous phase temperature, T , expressed in the gray scale are displayed. In the figure (b), the combustion reaction rate, R_F , expressed in the gray scale and the droplet location and diameter, D , are displayed simultaneously. In the

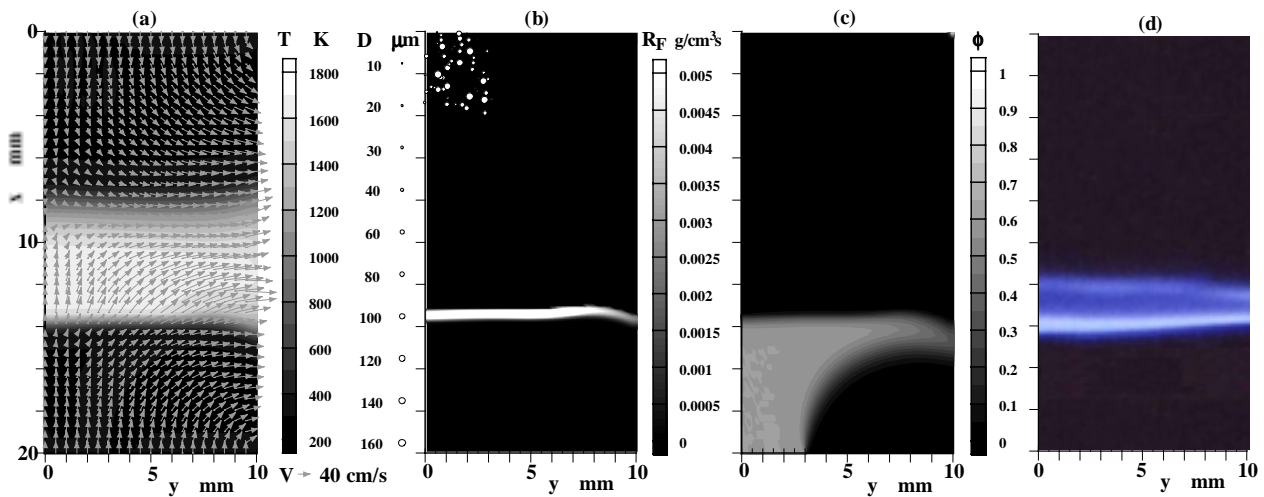


Fig. 3 Numerical results ($t = 5$ ms after spray injection) and the corresponding flame photograph

figure (c), equivalence ratio, ϕ , expressed in the gray scale is displayed and contours of the stoichiometric ($\phi = 1.0$) are described if there are. In the figure (d), trajectories of the droplets are visualized by an Ar-ion laser sheet in the flame photograph (only the large droplets are visualized due to low power of the laser sheet). The exposure time of the flame photographs is $1/15$ s.

In Fig. 3 at $t = 5$ ms after spray injection, very thin flame front (region of large R_F value) of the gaseous fuel supplied from the lower port is seen at around $x = 13.5$ mm (see the figure (b)). At this time step, no effect of the supplied droplet fuel on the gaseous flame is observed. The gaseous flame front locations of the experimental observation and the numerical result correspond very well each other to confirm validity of the present numerical code for calculating gaseous flames.

Figure 4 is for the results at $t = 25$ ms after spray injection. The gaseous flame shape is distorted due to intrusion of the fuel droplets and the large droplets penetrate into the reaction zone to reach the counter flow region. Combustion of single droplets and droplet groups occur in high temperature region of the gaseous flame in diffusion combustion mode. In the region, blue flames are observed in the corresponding photograph since the equivalence ratio, ϕ , is low. As seen in the figure (c), pre-vaporization of droplets occurs in approaching spray flow above the high temperature region. Pre-mixture, (which equivalence ratio is about 0.05) is generated to form a weak thin flame front burning in premixed combustion mode at around $x = 8.5$ mm. Of course, although the mixture of $\phi = 0.05$ is not inflammable, a premixed flame is sustained, in this case, by the heat from high temperature region of the diffusion flame. The vaporization of droplets in the high temperature region works as the source of fuel vapor for burning in diffusion-combustion mode.

In Fig. 5 at $t = 30$ ms, the combustion regions of single droplets and droplet groups seen at $t = 25$ ms get together to form a large droplet group with very large equivalence ratio. Luminous flames are observed in the photograph due to the increased equivalence ratio. The premixed combustion of pre-vaporized fuel becomes more intense owing to the increased amount of spray evaporation.

In Fig. 6 and 7 at $t = 35$ and 40 ms, respectively, the luminous flame region of a large droplet group becomes much larger. No combustion reaction occurs inside the large droplet group, and only the periphery is burning in diffusion combustion mode just outside of the contour of the stoichiometric ($\phi = 1.0$), which corresponds to the internal droplet group combustion mode⁽¹⁾. The premixed combustion region of pre-vaporized fuel becomes much more intense, where a continuous blue flame is observed in the corresponding flame photograph.

4. CONCLUSIONS

Numerical calculations and experimental observations of combustion processes of n-decane polydisperse spray entering gaseous flame front stabilized in laminar 2D counter flow configuration were conducted by the Eulerian/Lagrangian approach. For the disperse phase, all the individual droplets were tracked without using the concept of "droplet parcel". The results were compared to each other to ensure validity of the simulation model. Time evolution of burning processes of fuel spray entering high temperature region of the gaseous flame was discussed. As a result, twin flames of premixed combustion of pre-vaporized fuel and diffusion combustion of droplet groups were observed on the spray flow side.

REFERENCES

- (1) Chiu, H. H., et al., 19th Symp. (Int.) on Combust., (1982), 971, The Combust. Inst.
- (2) Akamatsu F. et al., Atomization and Sprays, **7**(1997), 199.
- (3) Mizutani, Y. et al., Mechanics and Combustion of Droplets and Sprays (Ed. H. H. Chiu and N. A. Chigier), (1996), 187, Begell house Inc. NY.
- (4) Akamatsu, F. et al., 26th Int. Symp. on Combustion, Combustion Institute (1996), 1723.
- (5) Takada, S. et al., Proc. of JSME Kansai, No.004-1 (2000-3), 5-37.
- (6) Kee, R. J., et al., SANDIA Report, SAND87-8215B (1987).
- (7) Kee, R. J., et al., SANDIA Report, SAND86-8246 (1986).
- (8) Abramzon, B. and Sirignano, W. A., ASME-JSME Thermal Eng. Joint Conf. (1987), Vol. 1, 11.
- (9) Patankar, S. V., Numerical Heat Transfer and Fluid Flow, (1985), McGraw-Hill.
- (10) Crowe, C. T., et al., Trans. ASME, J. of Fluids Eng., **99** (1977), 325.
- (11) Putnam, A. A., A.R.S. J., **31**(1969), p.1467.
- (12) Hubbard, G. L., et al., Int. J. Heat and Mass Transfer, **8**(1975), 1003.
- (13) Continillo, G. and Sirignano, W. A., Combustion and Flame, **8**(1990), 325.
- (14) Westbrook, C. K. and Dryer, F. L., Prog. Ener. Combust. Sci., **10** (1984), 1.